Neuron
Article

Two Ca^{2+}-Dependent Steps Controlling Synaptic Vesicle Fusion and Replenishment at the Cerebellar Basket Cell Terminal

Takeshi Sakaba[1,*]
[1]Research Group Biophysics of Synaptic Transmission, Max Planck Institute for Biophysical Chemistry, 37077, Göttingen, Germany
*Correspondence: tsakaba@gwdg.de
DOI 10.1016/j.neuron.2007.11.029

SUMMARY

Cerebellar basket cells inhibit postsynaptic Purkinje cells in a rapid and precise manner. To investigate the mechanisms of transmitter release underlying this rapid inhibition, Ca^{2+} uncaging was employed to measure the intracellular Ca^{2+} dependence of transmitter release and the kinetics of synaptic vesicle pool transitions in immature basket cell synapses at room temperature. Vesicle release properties distinct from those previously observed at excitatory synapses were seen, including a relatively high intracellular Ca^{2+} sensitivity of vesicle fusion, rapid vesicle pool mobilization with few reluctant vesicles, and vesicle replenishment driven by unusually high Ca^{2+} levels from both local and residual Ca^{2+} sources during action potential trains. These results suggest that inhibitory basket cell synapses are optimized for rapid and precise temporal and spatial Ca^{2+} coordination of synaptic vesicle fusion and replenishment, which may contribute to the unique physiology of inhibitory synaptic transmission, including phasic release during action potential trains and tonic release by residual intracellular Ca^{2+}.

INTRODUCTION

Short-term plasticity induced by presynaptic high-frequency stimulation is diverse among different types of synapses in the mammalian CNS, ranging from depression to facilitation (Zucker and Regehr, 2002; Stevens, 2003). Such diversity has an important consequence on information processing in the brain, because facilitation and depression of synaptic responses during a high-frequency train of action potentials (APs) operate as high-pass and low-pass filters between pre- and postsynaptic neurons, respectively (Abbott et al., 1997; Dittman et al., 2000). Both pre- and postsynaptic factors are known to determine the extent of short-term plasticity. At the presynaptic side, Ca^{2+} regulation of neurotransmitter release has been considered to be one of the crucial factors for short-term plasticity, in addition to the modulation of presynaptic AP waveforms (Geiger and Jonas, 2000) and Ca^{2+} channels (Borst and Sakmann, 1998; Forsythe et al., 1998; Cuttle et al., 1998). At excitatory synapses the local Ca^{2+} concentration ($[Ca^{2+}]$) at the transmitter release site, which rises to more than 5–10 μM following an AP, determines release probability of synaptic vesicles (Meinrenken et al., 2003). Release probability determines not only synaptic strength in response to a single AP but also the rate of consumption of the readily releasable pool (RRP) of synaptic vesicles and sets the extent of synaptic depression during subsequent stimuli. In addition to the local $[Ca^{2+}]$, residual bulk $[Ca^{2+}]$ following APs, which is much smaller in amplitude (less than a micromolar) and decays with a time course of several hundreds of milliseconds to seconds, is an important determinant for various types of short-term plasticity, such as facilitation, augmentation, posttetanic potentiation, and Ca^{2+}-dependent acceleration of vesicle replenishment (Zucker and Regehr, 2002).

In order to understand the mechanisms of transmitter release and short-term plasticity, it is essential to know their intracellular Ca^{2+} dependence. Ca^{2+} imaging provides useful information for the dependence of short-term plasticity on residual Ca^{2+}. However, the local $[Ca^{2+}]$ is difficult to measure, and even if it were possible to measure the local $[Ca^{2+}]$ (Llinas et al., 1992; Tucker and Fettiplace, 1995), the spatial arrangement between Ca^{2+} channels and Ca^{2+} sensors is uncertain. To probe the intracellular Ca^{2+} dependence directly, Ca^{2+} uncaging has been shown to be a useful method (Heidelberger et al., 1994; Rieke and Schwartz, 1996; Thoreson et al., 2004). Uniform elevation of $[Ca^{2+}]$ by flash photolysis allows one to establish the relationship between the kinetics of transmitter release and the intraterminal $[Ca^{2+}]$, which is reported by a Ca^{2+} indicator. In the mammalian CNS, however, this method has been limited to several large presynaptic terminals (Bollmann et al., 2000; Schneggenburger and Neher, 2000; Beutner et al., 2001), which are all glutamatergic. It is not known whether the $[Ca^{2+}]$ dependence obtained from these model systems is generalized. Transmitter release mechanisms may differ among synapses in order to adapt themselves to the specific tasks of signal transfer between neurons (Reyes et al., 1998). In the crayfish neuromuscular junction, it has been shown that the intracellular Ca^{2+} dependence differs between tonic and phasic synapses (Millar et al., 2005).

Here, the analysis of flash photolysis experiments was extended to smaller inhibitory presynaptic terminals of immature cerebellar basket cells. The basket cell terminals make collaterals to Purkinje cells and are involved in rapid feedforward inhibition from granule cells to Purkinje cells, limiting the time window of

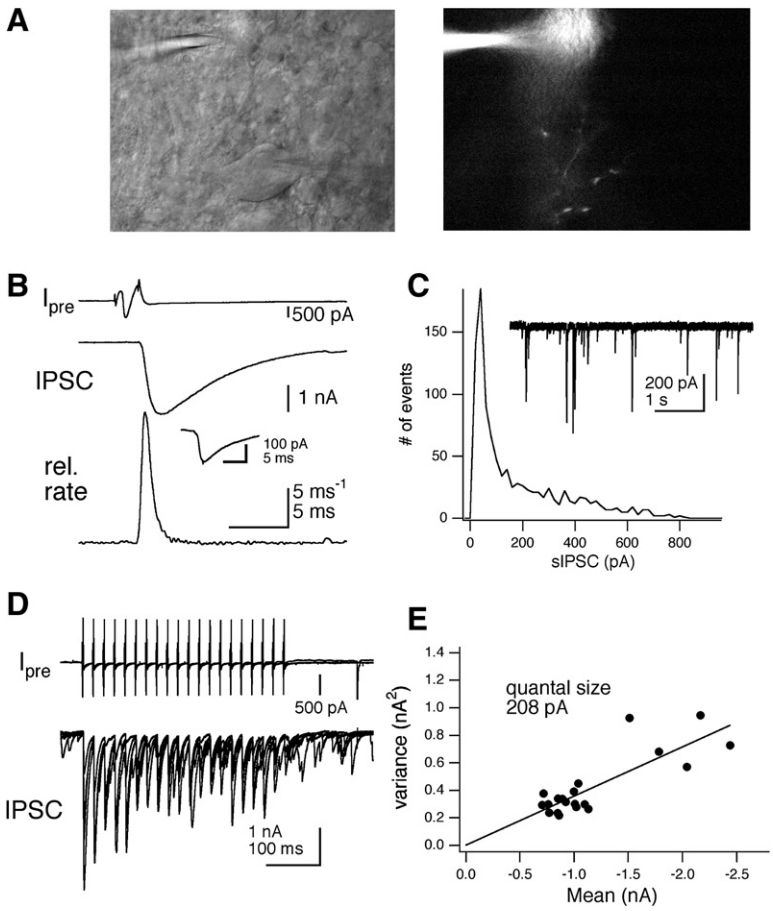

Figure 1. Properties of Synaptic Transmission between Mouse Cerebellar Basket and Purkinje Cells

(A) (Left panel) Transmission image of the slice preparation. Basket cell soma (top) is out of focus and therefore not visible. The connected Purkinje cell is shown below. (Right panel) Fluorescent image of the basket cell axon. The presynaptic patch pipette contained Fura-2FF. Terminals are seen close to the position of the Purkinje cell soma.

(B) Simultaneous recordings from a basket cell and a Purkinje cell. The presynaptic basket cell was depolarized from −80 mV to 0 mV for 2 ms, and a presynaptic AP was elicited during the pulse (top, presynaptic current). An AP-evoked IPSC (average of ten traces) was evoked at the postsynaptic Purkinje cell (middle). In the bottom trace, the release rate during a single AP estimated by the deconvolution method is shown. The inset shows the average mIPSC measured by eliciting an AP in low extracellular Ca^{2+} medium (0.6 Ca^{2+}/3 Mg^{2+}) in the same cell pair.

(C) An example of spontaneously occurring mIPSCs (inset) and the quantal distribution of mIPSCs recorded at the Purkinje cell.

(D) Twenty APs (50 Hz) were elicited at the basket cell (I_{pre}), which caused IPSCs (IPSC). Five responses are superimposed.

(E) Variance and mean of the IPSC amplitude in response to each AP during a train are plotted against each other. The slope of the line fit was 350 pA, which was further corrected for quantal dispersion of mIPSCs and the latency fluctuation of individual release events, yielding a quantal size estimate of 208 pA.

AP generation at the Purkinje cells in response to firing of granule cells (Mittmann et al., 2005). Although the size of the presynaptic terminals is smaller than that of the large glutamatergic terminals mentioned above, it is amenable to conventional fluorescent Ca^{2+} measurements (Llano et al., 1997; Forti et al., 2000). By infusing a caged Ca^{2+} compound and a Ca^{2+} indicator through a patch pipette positioned at the soma, the intracellular Ca^{2+} sensitivity of transmitter release as well as that of vesicle replenishment was determined. Unexpectedly, not only the transmitter release process itself but also the vesicle replenishment requires a high [Ca^{2+}].

RESULTS

Synaptic Transmission between Cerebellar Basket Cells and Purkinje Cells

Simultaneous whole-cell recordings were made from P11–16 mouse cerebellar basket cells and Purkinje cells in order to study GABAergic synaptic transmission, where physiological features have been well characterized (Vincent and Marty, 1996). As shown in Figure 1A, a basket cell sends an axon that forms collaterals to the soma of Purkinje cells (see also Figure S1 available online). The presynaptic basket cell was depolarized from a holding potential of −80 mV for a short period (to +0 or +40 mV for 2 ms) to cause an AP. An AP evoked an inhibitory postsynaptic current (IPSC) of several nanoamperes in amplitude at the postsynaptic Purkinje cell voltage clamped at −80 mV (Figure 1B). Because the presynaptic patch pipette contained high intracellular Cl^-, IPSCs were seen as inward currents throughout the experiment. An AP could also be caused by current injection under current-clamp mode, which caused an IPSC of similar amplitude (94% ± 13%, n = 5 cell pairs).

Three methods were used to estimate the quantal size. First, spontaneous mIPSCs in the presence of TTX were sampled (Figure 1C, inset). The mean mIPSC amplitude was 171 ± 22 pA (n = 6 cell pairs), and the histogram showed a skew toward larger values (Figure 1C), which yielded a CV of 0.86 ± 0.02 (n = 9). Second, single quanta were evoked by APs of the basket cell in the presence of low extracellular Ca^{2+} (0.6 mM Ca^{2+}/3 mM Mg^{2+}; Barrett and Stevens, 1972; Kraushaar and Jonas, 2000). In this experiment, 39% of the stimulation caused detectable IPSC (957/2423 trials in eight cell pairs). The inset of Figure 1B shows the average IPSC obtained from such a method in one cell pair. The quantal size was estimated to be 151 ± 150 pA (SD). Third, in order to estimate quantal sizes during heavy use of the synapse, a high-frequency train of APs (50 Hz × 20) was repeated 20 to 80 times with an interval of 10 s, and nonstationary fluctuation analysis was applied (Scheuss et al., 2002). The AP train usually caused a slight synaptic depression of synchronous release followed by asynchronous release during and after the train

(Figure 1D). On average, asynchronous release during the train was less than 20% of the initial amount of synchronous release during the first AP in the train (see Figure S6). Variance and mean of each AP-evoked IPSC amplitude during the train were calculated and plotted against each other as shown in Figure 1E. Because the variance-mean plot (Figure 1E) showed a linear relationship, quantal sizes were constant during a stimulus train. From the slope of the fit, quantal sizes were estimated to be 149 ± 29 pA (n = 5 cell pairs). Therefore, three quantal size estimates had a similar value of ~150 pA. The observation that the three estimates matched and that the variance-mean plot was linear shows that postsynaptic mechanisms, such as receptor saturation and desensitization, do not occur strongly during repetitive stimulation (Auger and Marty, 2000).

Given constant quantal sizes, synaptic currents can be assumed to be a product of the convolution between the quantal current and quantal release rates, and therefore, quantal release rates can be calculated by the deconvolution method. The bottom trace of Figure 1B shows the release rate observed during a single AP, which had a peak amplitude of 15 vesicles ms^{-1} and a half-width of 1 ms.

The Number of Readily Releasable Vesicles Measured by Ca^{2+} Uncaging

Synaptic strengths are determined by the product of vesicular release probability and the number of readily releasable synaptic vesicles. Depletion of the RRP during repetitive stimulation depresses subsequent synaptic responses. In contrast, a large pool of vesicles together with low release probability allows facilitation of synaptic responses (Zucker and Regehr, 2002). In order to measure the RRP size accurately, it is desirable to deplete the pool in a short time, as slow vesicle pool depletion may be balanced by overlapping vesicle replenishment, resulting in an inaccurate estimate of the pool size. To stimulate transmitter release rapidly, basket cells were dialyzed with the caged Ca^{2+} compound DM-nitrophen and the Ca^{2+} indicator dye Fura-2FF. Within 2–5 min of whole-cell dialysis, the compounds reached the presynaptic terminal sufficiently as judged by fluorescence intensity (Figure 1A). Under this condition, transmitter release can be evoked either by Ca^{2+} influx via Ca^{2+} channels activated by a presynaptic AP or else by uncaging of the caged Ca^{2+} compound using short pulses of UV light, which thereby liberates free Ca^{2+} throughout the presynaptic terminal. Since DM-nitrophen strongly buffers Ca^{2+}, external Ca^{2+} was elevated to 10 mM to restore transmission. Under this condition, synaptic responses evoked by presynaptic APs showed a pronounced depression and reached a steady state during a 50 Hz train (Figure 2A, see Figure 5C for a summary plot). Then, flash photolysis was performed in the same cell pair (Figure 2B), which elevated the $[Ca^{2+}]$ from the basal level to 15 μM. A phasic IPSC of 10 nA in amplitude was evoked at the postsynaptic Purkinje cell in response to the rapid elevation of $[Ca^{2+}]$ at the presynaptic terminals. Following the phasic component, a sustained component of randomly occurring IPSCs continued as long as $[Ca^{2+}]$ remained high. When five APs were applied following the flash (Figure 2B), IPSCs in excess of the randomly occurring ones were minimal, indicating that flash photolysis and APs drew from the same pool of vesicles.

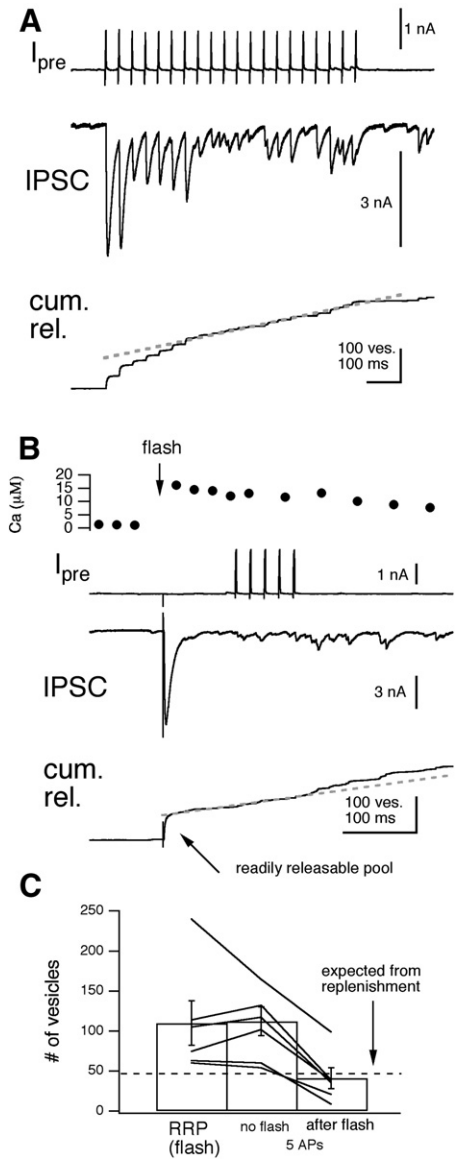

Figure 2. Ca^{2+} Uncaging at the Basket Cell Synapse

(A) A train of APs (50 Hz × 20) was applied to the basket cell, and an IPSC was recorded at the Purkinje cell. From the IPSC, the cumulative release was estimated by the deconvolution method. Extracellular Ca^{2+} was 10 mM. Dotted line indicates the line fit to the steady-state.

(B) Flash-evoked release. From top, intraterminal Ca^{2+} concentration, presynaptic current, IPSC, and cumulative release estimated from the deconvolution method are shown. Five APs were elicited at the basket cell following the flash. The gray dotted line indicates the line fit of the sustained component. The same cell pair as in (A).

(C) The panel shows the cumulative amounts of release evoked by flash photolysis (left), five APs (middle), and five APs following flash photolysis (right). The dotted line indicates the amount of release expected from a vesicle recruitment rate of 0.4 ms^{-1}.

Error bars represent SEM.

Using the deconvolution method, the amount of release following flash and/or APs was quantified. In order to estimate the RRP size, the sustained component of release was fitted by a line

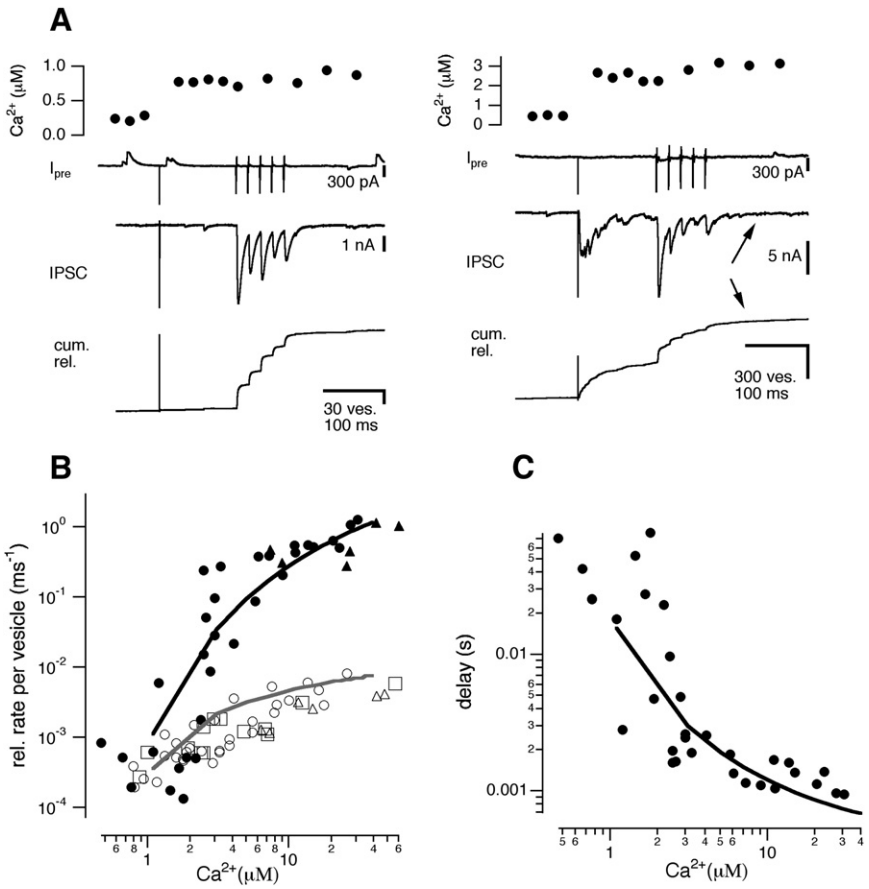

Figure 3. The Intracellular Ca^{2+} Dependence of Transmitter Release Rates at the Basket Cell Synapse

(A) Similar to Figure 2B, but the presynaptic [Ca^{2+}] was elevated to 0.8 (left) and 3 μM (right) following flash photolysis. From top, presynaptic [Ca^{2+}], presynaptic current, IPSC, and cumulative release are shown. In these examples, the intracellular [Ca^{2+}] was measured by Fura-4F. Arrows indicate the time points where vesicle replenishment rate was measured.

(B) The relationship between [Ca^{2+}] and the peak release rate per vesicle (the release rate normalized to the RRP size) evoked by flash photolysis is plotted as filled symbols. The relationship between [Ca^{2+}] and the rate constant of vesicle replenishment (normalized to the RRP size) is plotted as open symbols. Triangles represent the data in the presence of a low-affinity $GABA_A$ receptor antagonist TPMPA (300 μM) in the extracellular medium. Open squares represent the sustained rate evoked by flash photolysis following ten APs (Figure S3). Black line indicates expectations for the peak release rate per vesicle from the five-site sequential model of secretion. Grey line indicates the expectation from the same model, but for vesicle replenishment.

(C) The relationship between [Ca^{2+}] and delay of onset of release (when three vesicles have been released) after application of flash photolysis. Black line indicates expectations from the five-site model.

(Figure 2B, gray dotted line). This line was back extrapolated to the time point of the flash, resulting in an average pool size of 110 ± 28 vesicles in this particular set of experiments. From the slope of the line fits, the rate of vesicle replenishment was estimated to be 0.43 ± 0.11 vesicle ms^{-1}, equal to a time constant of 300 ± 57 ms. When the amounts of release during a 100 ms interval of stimulation (five APs) with and without preceding flash photolysis were compared, flash photolysis reduced the cumulative release to 35% ± 4%. The remaining release could be explained mostly by the replenishment (Figure 2C, dotted line), Furthermore, the cumulative amount of release during five APs and that of flash-evoked release (phasic component) were comparable on average (Figure 2C). Therefore, the RRP is depleted by the initial five APs, and the steady state after depression is presumably mediated by vesicle replenishment. Furthermore, the number of reluctant synaptic vesicles, which are not released by an AP but by flash, is not significant, unlike some glutamatergic synapses (Moulder and Mennerick, 2005; Wadel et al., 2007; Figure S3).

Intracellular Ca^{2+} Dependence of Vesicle Fusion and Replenishment at the Basket Cell Terminal

Next, we examined the intracellular Ca^{2+} dependence of transmitter release. In this experiment, flash photolysis of different intensity was applied. 130 ms following the flash photolysis, five APs were applied to deplete the remaining RRP. Figure 3 shows postsynaptic responses evoked by [Ca^{2+}] steps to different levels. In the left panel of Figure 3A, a [Ca^{2+}] rise from basal level to less than 1 μM elicited only two mIPSCs. Five APs following the flash still evoked large IPSCs. In contrast, a [Ca^{2+}] rise to 3 μM already elicited a fast-rising IPSC with amplitude of ~5 nA (right panel). A higher [Ca^{2+}] step to 15 μM elicited release more synchronously (Figure 2B). Figures 3B and 3C show a summary of the experiments plotting peak release rates per vesicle and delays of secretion after flash photolysis against [Ca^{2+}] (filled circles). Peak release rates per vesicle were calculated by dividing the peak flash-evoked release rate by the size of the RRP (221 ± 36 vesicles from 23 cell pairs). The RRP was approximated by the cumulative amount of release until the end of five APs when flash intensity was weak. A very steep Ca^{2+} dependence of release rates was observed between 1 and 5 μM, which became shallower afterward (Figure 3B, closed symbols). At high [Ca^{2+}], the release rate constant became close to 1 ms^{-1}. To examine whether postsynaptic receptor saturation affects the release rate estimates after a strong flash, a low-affinity $GABA_A$ receptor antagonist, TPMPA (300 μM), was applied, which reduced an AP-evoked IPSC to 30% ± 4.1% (n = 3 cell pairs). The data are shown as filled triangles in Figure 3B, showing little difference from control data sets (n = 5 cell pairs). Synaptic delays after flash photolysis also depended on [Ca^{2+}], approaching 1 ms

around 20–30 μM (Figure 3C). Therefore, GABA release can be fast at high [Ca^{2+}].

The intracellular Ca^{2+} sensitivity of the sustained component of release, which presumably reflects vesicle replenishment, was also measured by fitting the time course of cumulative release by a straight line (Figure 2B and Figure S2). When flash elevated [Ca^{2+}] to a relatively low level, the rate was measured after five APs where the RRP was emptied (see arrows in Figure 3A). Sustained rate was then normalized to the RRP to obtain the rate constant. As shown in Figure 3B (open circles), the vesicle replenishment rate constant had a shallow dependence on [Ca^{2+}] compared with the phasic component of release. The time constant of vesicle replenishment varied from several seconds to hundreds of milliseconds, depending on the intracellular [Ca^{2+}]. In an additional set of experiments (Figure S3), flash photolysis was applied after ten APs, which were enough to deplete the RRP (Figure 2). The measured rate of the sustained component was also plotted in Figure 3B (open squares), which overlapped with open circles.

In order to quantify the intracellular [Ca^{2+}] sensitivity of phasic and sustained components of release, a model of synaptic vesicle fusion was introduced (see Experimental Procedures for a model). For phasic release, the model assumes sequential binding of Ca^{2+} to the release machinery, with Ca^{2+}-dependent forward and Ca^{2+}-independent backward rates. In addition, a final Ca^{2+}-independent irreversible step was assumed. In order to fit a nonlinear relationship at the low-end of the dose-response curve, five Ca^{2+}-binding steps were necessary. Ca^{2+} binding, Ca^{2+} unbinding, and final rates for release were estimated to be 9×10^7 $M^{-1}s^{-1}$, 3000 s^{-1}, and 5000 s^{-1}, respectively (Figures 3B and 3C, black lines). For vesicle replenishment, one Ca^{2+}-dependent priming step, followed by a Ca^{2+}-independent step of filling the RRP, was assumed. In Figure 3B, the Ca^{2+} binding rate and unbinding rates were estimated to be $k_{prim} = 5 \times 10^6$ $M^{-1}s^{-1}$ and k_{unprim} = 50 s^{-1}, respectively. This yields Kd of 10 μM for Ca^{2+}, meaning a relatively low affinity.

Intracellular Ca^{2+} Concentration at the Release Site during an AP

Because local [Ca^{2+}] at the release site is difficult to measure by microscopic methods (Neher, 1998), a back-calculation approach was employed instead. Given the release model as constructed in Figure 3 and release rates as measured during an AP, the time course of [Ca^{2+}] at the release site during an AP can be obtained by calculating the inverse function of the release model (Bollmann et al., 2000; Schneggenburger and Neher, 2000). As has been shown in Figure 1B, release rates during an AP had a peak amplitude of 15 ms^{-1} and a half-width of 1 ms (Figure 4B, data). Then, various amplitudes and time courses of [Ca^{2+}] were entered into the release model until the release time course during an AP was perfectly predicted by the release model (Figure 4B, model). When estimating the [Ca^{2+}], the RRP size must be known. When the average size from the flash experiments was used (221 ± 36 vesicles), the intracellular [Ca^{2+}] at the release site was estimated to rise to 20 μM with a half-width of 0.5 ms during an AP (Figure 4A). On average, [Ca^{2+}] at the release site is estimated to have a peak amplitude of 20.9 ± 3.1 μM and a half-width of 503 ± 61 μs (n = 6 cell pairs).

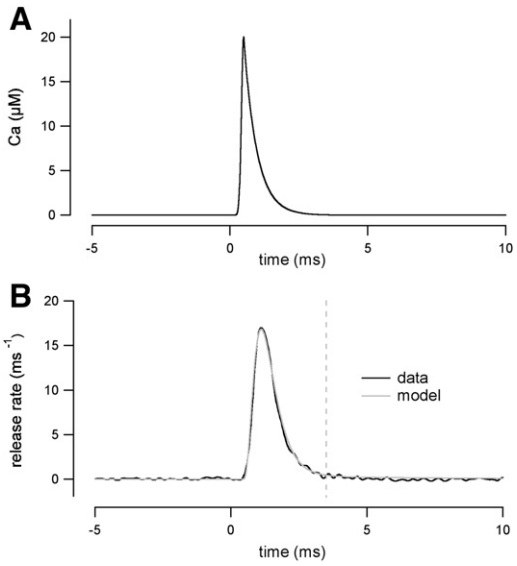

Figure 4. Estimation of an AP-Evoked Ca^{2+} Transient at the Transmitter Release Site

[Ca^{2+}] at the transmitter release site (A) was estimated from the release rate shown in (B) (solid line). The gray trace in (B) shows a model calculation of the release rate. The dotted line separates synchronous and asynchronous release (see Figures 5 and 6).

Mechanisms of Short-Term Synaptic Depression and Recovery during a 50 Hz Train

In addition to an AP-evoked release, vesicle replenishment also requires relatively high [Ca^{2+}] (Figure 3B). During an AP train (Figure 2A), the steady state after depression must be mediated by vesicle replenishment, because most of the RRP should have been depleted by the first five APs (Figure 2C). By fitting a line during the steady state and comparing it with the RRP size (Figure 5A), the time constant of vesicle replenishment during an AP train was estimated to be 373 ± 68 ms (n = 6 cell pairs), which corresponds to a rate constant of 0.0027 ms^{-1}. The comparison with the intracellular [Ca^{2+}] dependence of the replenishment rate shown in Figure 3B indicates that continuous elevation [Ca^{2+}] to 5–10 μM is necessary for attaining the rate constant of 0.003 ms^{-1} (Figure S4), implying the involvement of local [Ca^{2+}] close to Ca^{2+} channels. Below, we examined more closely whether the vesicle depletion and replenishment mechanisms as shown in Figure 3 were sufficient to explain synaptic depression.

If facilitation exists at the basket cell-Purkinje cell synapse, the facilitation process needs to be implemented in the transmitter release model. In order to reveal facilitation from overlapping depression, release probability was calculated by dividing the amount of release by the RRP size at each time point during an AP train. Figure 5A shows the average time course of cumulative release during a 50 Hz train from the experiment of Figure 2 (10 mM extracellular Ca^{2+} and DM-nitrophen in the patch pipette). The RRP size was calculated by simulation, which assumed a vesicle replenishment rate proportional to the reduction of the RRP size at a given time. It was further assumed that either

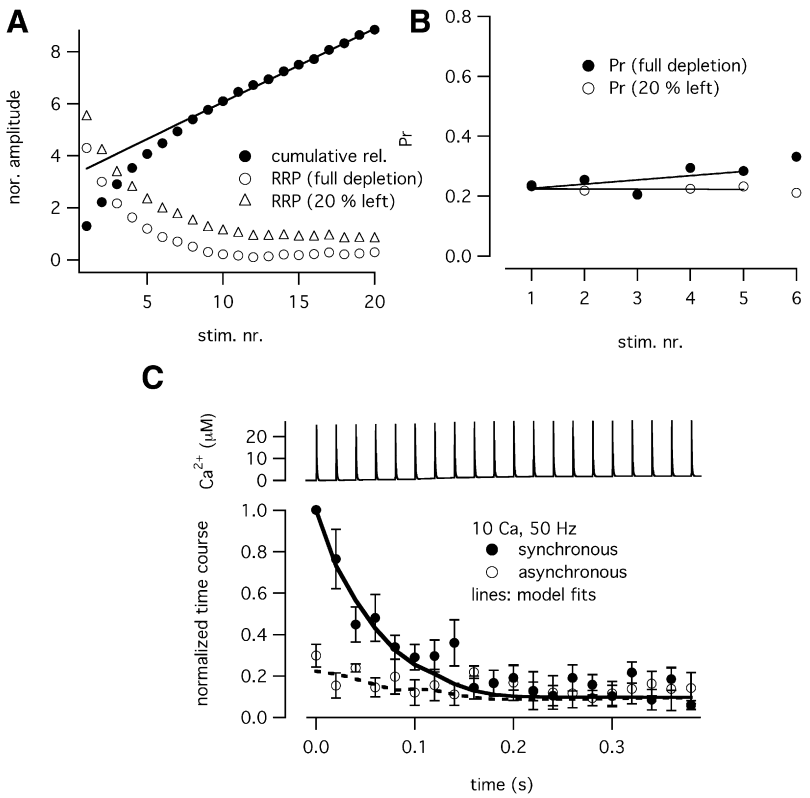

Figure 5. Release Probability and the Time Course of Synaptic Depression in 10 mM Extracellular [Ca^{2+}]

(A) Cumulative release during an AP train (50 Hz) is plotted as a function of stimulus number (filled circles). The data were obtained in the set of experiments shown in Figure 2 and carried out in the presence of 10 mM extracellular Ca^{2+}. Cumulative release was normalized to the response evoked by the first AP in the train and was averaged over six cell pairs. A line was fitted to the last five responses to estimate the release rate during the steady state. A model assuming a single vesicle pool depletion and a single time constant for replenishment is constructed to estimate the remaining pool size from original data. Open circles assume that the RRP becomes empty at the steady state during an AP train, whereas open triangles assume that the RRP becomes 20% of the initial value at the steady state.

(B) Release probability estimated from the model calculation assuming full vesicle pool depletion (filled circles) and 20% remaining at the steady state (open circles). Data are limited to the first five APs because the estimate becomes unreliable when the remaining RRP size becomes small.

(C) Synaptic depression in the presence of 10 mM extracellular Ca^{2+}. Filled and open circles show the amount of synchronous and asynchronous release in each AP during a train. The data are normalized to the amount of synchronous release evoked by the first AP in the train. Solid and dotted lines represent the model prediction of the amounts of asynchronous and asynchronous release, respectively. The model assumes that transmitter release and vesicle replenishment rates are driven by the same [Ca^{2+}] waveform shown in the top.

Error bars represent SEM.

(1) RRP becomes empty during the steady state or that (2) RRP becomes 20% of the initial value at the steady state (Figure S3). Because the estimates of release probability become unstable when the remaining pool size becomes small, the analysis was restricted to the first five APs. As shown in Figure 5B, release probability (~0.25) stayed constant during this period. As a second approach to reveal facilitation, the extracellular [Ca^{2+}] was lowered to 1 mM (without DM-nitrophen in the patch pipette). As shown in Figure S6, IPSCs did not show significant facilitation. It was concluded that facilitation is not significant, and the following model simulation will not take the facilitation process into account.

For simulating the time course of synaptic depression using the release model, the following assumptions have been made. For simplicity, the same [Ca^{2+}] waveform was used to drive secretion and vesicle replenishment. The [Ca^{2+}] waveform was the same as in Figure 4, but the peak amplitude was set to 25 μM in order to obtain a release probability of 0.22 (Figure 5B) during an AP. The same [Ca^{2+}] waveform was repeated at 50 Hz (Figure 5C, top). Furthermore, slowly rising [Ca^{2+}] was superimposed to explain asynchronous release, which was 20% of the amount of synchronous release in the beginning but persisted in a similar level during a train (Figure 5C, open symbols). Asynchronous release was determined as release events after the dotted line in Figure 4B (3 ms after the start of synchronous release). Slow elevation of the intracellular [Ca^{2+}] to 1–2 μM was estimated to evoke the asynchronous release rate observed in Figure 5C. The lines of Figure 5C show the estimated time course of synchronous (solid) and asynchronous release (dotted) during an AP train, which fit relatively nicely with the experimental data. Therefore, the model assuming the same local [Ca^{2+}] waveform for both vesicle fusion and vesicle replenishment explains the time course of synaptic depression during an AP train (see also Figure 6 and Figure S6).

[Ca^{2+}] in the terminal returns quickly to a submicromolar level after closure of presynaptic Ca^{2+} channels (Neher, 1998). Residual bulk [Ca^{2+}] after an AP train was relatively small (<1 μM from Figure S5), which caused a replenishment rate constant of <1 s^{-1} (Figure 3B). Therefore, recovery from synaptic depression after an AP train would be expected to be slow. This expectation was tested in Figure 6A. The extracellular [Ca^{2+}] was elevated to 5 mM in order to observe clear synaptic depression. During an AP train, IPSCs showed depression and reached a steady state (dotted line), which was ~20% of the initial value (filled circles in Figure 6B for the average depression time course of synchronous release from ten cell pairs). After the train of APs, six APs were applied with varied intervals to monitor the recovery from depression (Figure 6A). When the initial five responses were compared between the first and the second stimulus train, the recovery time course could be fitted with a single exponential of 1.7 s (Figure 6C). This time constant was four to five times slower than the replenishment rate during an AP train (300–400 ms,

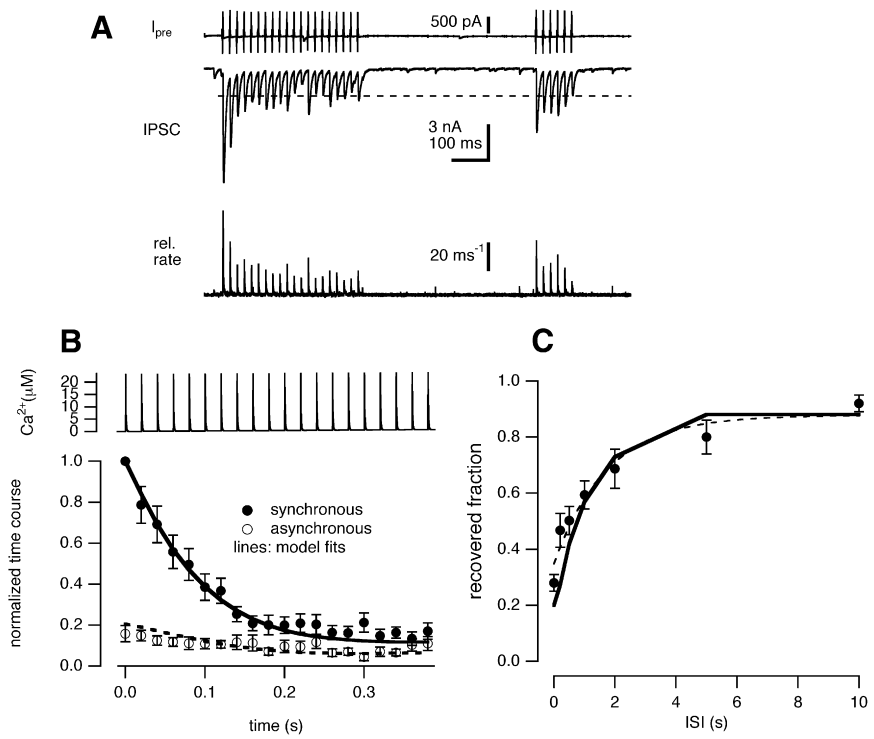

Figure 6. The Time Course of Synaptic Depression and Recovery

(A) This set of experiments was carried out in the presence of 5 mM extracellular Ca^{2+} (without DM-nitrophen in the pipette). A train of APs (50 Hz × 20) was followed by the second train (50 Hz × 6) with an interval of 500 ms. From top, presynaptic current, postsynaptic IPSC, and the release rates estimated from the deconvolution method are shown. The dotted line in the IPSC trace shows the steady-state level during the first train.

(B) The same as Figure 5C, but the time course of synchronous and asynchronous release from the experiment of (A) is shown. The data are normalized to the amount of synchronous release during the first AP in a train. Lines indicate the prediction from the release model using the $[Ca^{2+}]$ waveform shown in the top as input.

(C) Time course of recovery from synaptic depression. The data are pooled from the experiment shown in (A), with varied intervals between the two trains. The amounts of release during the initial five APs in the train (synchronous + asynchronous release) were compared. Filled circles represent the data, and the dotted line was an exponential fit to the data with a time constant of 1.7 s. The solid line indicates the model prediction.

Error bars represent SEM.

Figure 2). In order to examine whether vesicle fusion and replenishment rates as seen in Figure 3 could explain synaptic depression and recovery, the release model was applied to the case of Figure 6. In Figure 6B, it was assumed that each AP caused an elevation of local $[Ca^{2+}]$ to 23 μM, which decayed with a time constant of 0.5 ms. The same $[Ca^{2+}]$ waveform was assumed to drive both vesicle fusion and replenishment. After the train, residual $[Ca^{2+}]$ was assumed to be at a low level, as seen in Figure S5. The model captured both depression (Figure 6B, straight line) and recovery time courses (Figure 6C, straight line). In order to explain the amount of asynchronous release during a train, a slow elevation of $[Ca^{2+}]$ to 1 μM had to be assumed (dotted line, Figure 6B).

The Effects of Synaptobrevin Cleavage on Transmitter Release at The Basket Cell Synapse

It has been shown that the deficiency of synaptobrevin slowed recovery from synaptic depression at glutamatergic synapses of the hippocampus and the calyx of Held (Deak et al., 2004; Sakaba et al., 2005). We examined whether this is also the case for the basket cell synapse by infusing botulinum neurotoxin B (BoNT/B) and tetanus toxin (TeNT). Although BoNT/B and TeNT cleave synaptobrevin at the same site, BoNT/B is supposed to cleave trans-SNARE complexes, in contrast to TeNT, which only cleaves free, monomeric synaptobrevin (Pellizzari et al., 1996). In Figure 7A, the experiment was similar to Figure 6, but BoNT/B (3 μM) was introduced into the basket cell soma. The toxin caused inhibition of transmitter release evoked by an AP train within 5 min, as summarized in Figure 7B (n = 7 cell pairs). TeNT (6 μM) blocked IPSCs similarly (Figure 7B, n = 5 cell pairs). Figure 7C shows the average time course of release during a 50 Hz AP train. Open and filled circles show the time course of release immediately after whole-cell rupture and when the first IPSC becomes 40% of the initial value, respectively. Grey traces show the time course of synaptic depression of the latter condition normalized to the first IPSC in the train, illustrating that both TeNT and BoNT/B blocked release without changing the time course of depression significantly. As seen in Figure 7D, the recovery from synaptic depression was not affected by the toxins.

From Figure 7, synaptobrevin cleavage seems to block release in an all-or-none manner without altering the kinetics of release and vesicle replenishment (steady-state level after depression). However, it remained possible that the Ca^{2+} sensitivity for release might have been affected by the toxins at a low Ca^{2+} level, because APs test only Ca^{2+} sensitivity during short impulses of high $[Ca^{2+}]$ (20–30 μM). In order to probe the intracellular Ca^{2+} sensitivity for release over a wider range, flash photolysis experiments were carried out, which revealed an interesting difference between BoNT/B and TeNT. In each cell pair, flash photolysis was applied once the toxins inhibited an AP-evoked release to more than 50% of the initial value. On average, the number of readily releasable vesicles under BoNT/B and TeNT was 36 ± 6 vesicles (n = 27 flash responses from 17 cell pairs) and 91 ± 29 vesicles (n = 28 responses from 14 cell pairs), respectively, whereas it was 228 ± 40 vesicles in the control (n = 32 responses). In Figure 8A, flash photolysis elevated the intracellular $[Ca^{2+}]$ to 5 μM in the presence of BoNT/B, which evoked only a few mIPSCs, while subsequent APs still caused release. In contrast, a similar elevation of $[Ca^{2+}]$ elicited phasic transmitter release in the presence of TeNT (Figure 8B). Subsequent five APs caused little release, indicating depletion of the RRP.

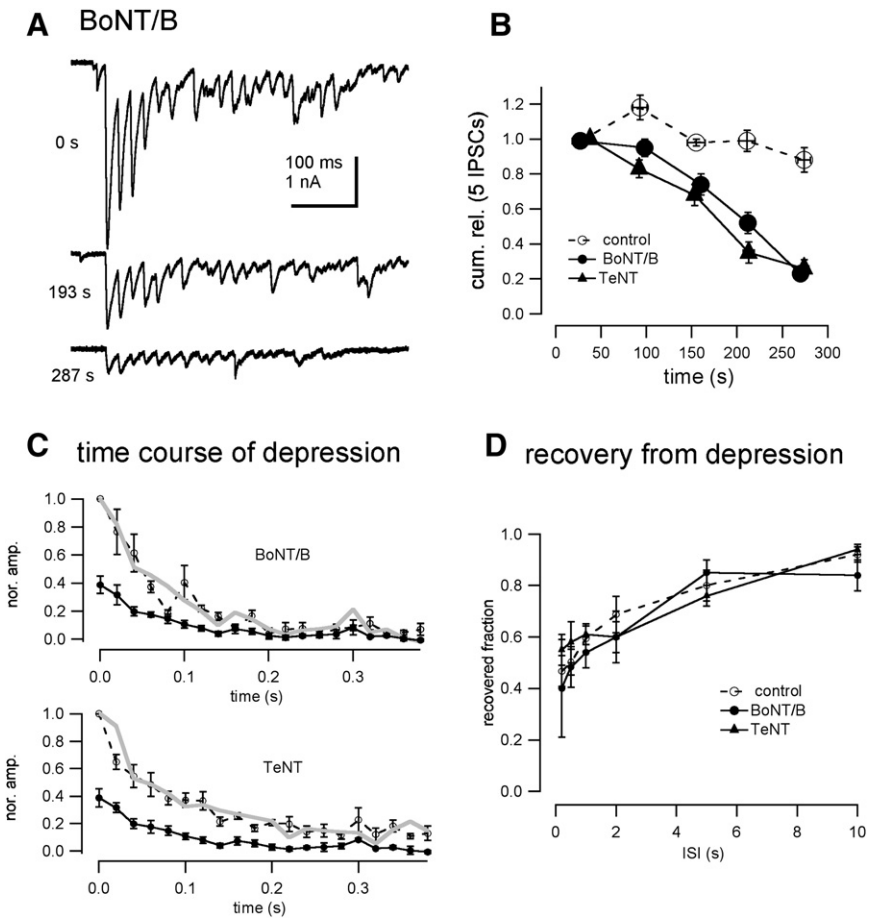

Figure 7. The Effects of Synaptobrevin Cleavage on Synaptic Responses

(A) BoNT/B (3 μM) was included in the presynaptic patch pipette. A train of APs (50 Hz × 20) was applied to examine the effect of the toxin on synaptic responses. Synaptic responses with various time points after whole-cell dialysis are shown. 5 mM Ca^{2+} was added in the extracellular medium.

(B) Time course of block of transmitter release. Cumulative release after the initial five APs during the train was plotted against the time after whole-cell recording. Open symbols indicate the control data sets, and filled circles and triangles indicate the data in the presence of BoNT/B (3 μM) and TeNT (6 μM) in the presynaptic patch pipette, respectively.

(C) The time course of synaptic depression during an AP train in the presence of toxins. Open circles connected by the dotted line show the time course of synaptic depression (synchronous release) obtained immediately after the whole-cell rupture. The data are normalized to the first IPSC. Filled circles connected by line show the data when the first IPSC during an AP train becomes ~40% of the initial value during whole-cell dialysis. Grey lines show the same data normalized to the first IPSC to illustrate the effect of the toxins on the time course of synaptic depression. The data obtained in the presence of BoNT/B (top) and TeNT(bottom) are shown.

(D) Recovery from synaptic depression. The same experiment as in Figure 6A was carried out in the presence of BoNT/B (filled circles) and TeNT (filled triangles). Open circles represent control data sets.

Error bars represent SEM.

Figure 8C shows the intracellular $[Ca^{2+}]$ dependence of the peak release rate per vesicle (left panel) and delay of secretion (right panel) in the presence of BoNT/B. Compared to the control condition (open circles), the dose-response curve was shifted rightward, indicating a change in the intracellular Ca^{2+} sensitivity. When the release model was used to fit the data, the Ca^{2+}-unbinding rate had to be increased more than 5-fold (3000 s^{-1} to 16,000 s^{-1}) without altering other parameters. In the presence of TeNT, the dose-response curve showed a less pronounced shift compared with BoNT/B or was indistinguishable from control data sets (Figure 8D). For model fitting, the Ca^{2+}-unbinding rate had to be increased less than 2-fold (3000 s^{-1} to 5000 s^{-1}). The rate of vesicle replenishment, which was measured by the sustained component of release after flash photolysis, showed a similar $[Ca^{2+}]$ dependence with and without toxins (Figure 8E), consistent with Figure 7D.

DISCUSSION

Here, inhibitory transmitter release was stimulated directly using flash photolysis at presynaptic terminals of cerebellar basket cells. Flash photolysis and an AP train released the same number of synaptic vesicles (Figure 2). Although transmitter release could be seen at a relatively low level of $[Ca^{2+}]$ (1–3 μM), the local $[Ca^{2+}]$ at the release site must be elevated to a high level (20 μM) for a short period (decay time constant of 0.5 ms) during an AP. Together with minimized short-term plasticity that is driven by residual bulk Ca^{2+} and has a long-lasting effect as well as the requirement of high $[Ca^{2+}]$ for vesicle replenishment, the basket cell synapse in P11–16 mice is adapted to rapid sensing of Ca^{2+} signals during an AP train. Additionally, cleavage of synaptobrevin has a different effect compared to other synapses, showing no effect on the vesicle replenishment process. Finally, BoNT/B and TeNT affect the intracellular Ca^{2+} dependence of release differently.

Intracellular Ca^{2+} Sensitivity of Transmitter Release at the Basket Cell Synapse

A high-affinity Ca^{2+} sensor (micromolar order) has been reported in inhibitory GABAeric synapses (Frerking et al., 1997; Kirischuk and Grantyn, 2002, 2003; Kirischuk et al., 1999) as well as neuromuscular junctions (Angleson and Betz, 2001) by examining the intracellular Ca^{2+} dependence of asynchronous and spontaneous release rates. These studies, however, did not cover the high $[Ca^{2+}]$ range, which is relevant for AP-evoked release. The present study indicates that the synchronous release mechanism has a lower affinity for Ca^{2+} (30 μM, by comparing binding and unbinding rate at zero basal Ca^{2+}). When Ca^{2+} binding and unbinding rates as well as final fusion rates are compared among the synapses where flash photolysis has been used for

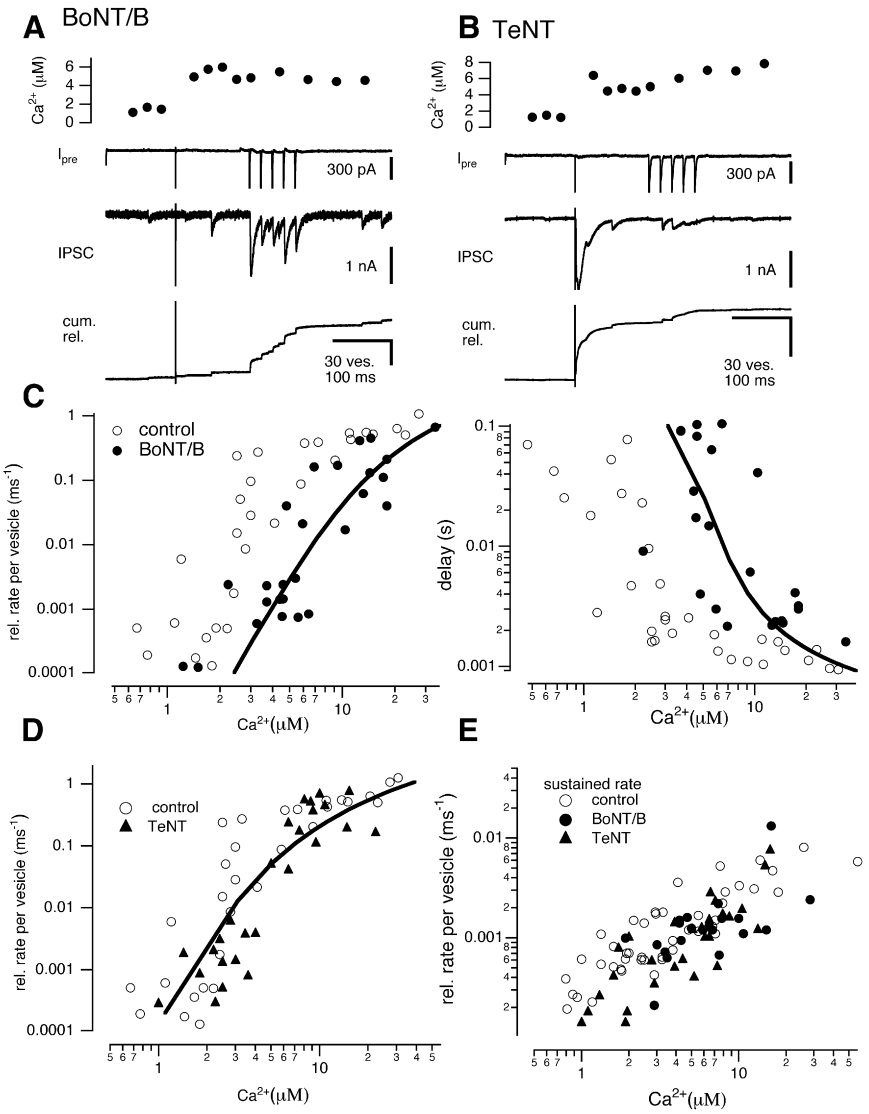

Figure 8. The Intracellular [Ca^{2+}] Dependence of Transmitter Release in the Presence of Botulinum and Tetanus Toxins

(A and B) Similar to Figure 2B, but the experiments were carried out in the presence of BoNT/B (A) and TeNT (B). From top, presynaptic [Ca^{2+}], presynaptic current, IPSC, and cumulative release are shown.

(C) The relationship between [Ca^{2+}] and the peak release rate per vesicle (left) and the delay of secretion (right) was obtained by flash photolysis. Open and filled circles represent control data sets and the ones in the presence of BoNT/B, respectively. Solid lines indicate the model prediction.

(D) Same as (C), but in the presence of TeNT (filled triangles) compared with control (open circles).

(E) The relationship between [Ca^{2+}] and vesicle replenishment rate (normalized to the RRP size). Open circles, filled circles, and triangles represent control data sets and the data in the presence of BoNT/B and TeNT, respectively.

determining Ca^{2+} sensitivity, the basket cell synapse has the lowest value of Ca^{2+}-unbinding rate, yielding a relatively high affinity for Ca^{2+} (Heidelberger et al., 1994; Beutner et al., 2001; Schneggenburger and Neher, 2000; Bollmann et al., 2000). This means that the low end of the dose-response curve extends to lower Ca^{2+} levels and that significant rates of release (comparable to asynchronous release rates during an AP train; Figure 5) occur at 1–3 μM [Ca^{2+}]. Although the affinity for Ca^{2+} is low, this study is, therefore, still consistent with the findings that GABA release is highly Ca^{2+} sensitive (Frerking et al., 1997; Kirischuk and Grantyn, 2003). It has been suggested that the mechanism of asynchronous release differs from that of synchronous release (Goda and Stevens, 1994; Maximov and Südhof, 2005). In Figures 5 and 6, the analysis assumed that synchronous and asynchronous release are mediated by the same release mechanism determined in Figure 3 and draw from the RRP (Hagler and Goda, 2001; Otsu et al., 2004), which explained the data nicely. The present study, however, did not cover the intracellular [Ca^{2+}] below 500 nM because spontaneous inputs from the interneurons other than the recording one might bias the estimation of release rates close to resting [Ca^{2+}]. Therefore, it remains as a possibility that a distinct release mechanism may operate at a very low Ca^{2+} level. In addition, separate asynchronous release mechanisms may exist at other synapses where copious asynchronous release is observed (Lu and Trussell, 2000; Hefft and Jonas., 2005).

The deconvolution method showed that the time course of release in response to an AP is very short (within milliseconds) at the basket cell synapse. To achieve such a fast time course, local [Ca^{2+}] must be elevated to 20 μM (Figure 4). Residual bulk [Ca^{2+}] evoked by an AP is more than 20-fold smaller (for response to an AP train, see Figure S5). Such a small amplitude of residual [Ca^{2+}] is insufficient to cause robust facilitation of transmitter release in the subsequent stimuli because the Ca^{2+} cooperativity is low at >10 μM [Ca^{2+}], and summation of residual Ca^{2+} to the local Ca^{2+} (Katz and Miledi, 1968) is ineffective to cause facilitation. Indeed, facilitation of release was not significant at the basket cell synapse (Figure 5 and Figure S6). Thus, the present study provides a mechanistic explanation of how the basket cell synapse minimizes short-term facilitation. This study is compatible with the finding that the knockout of parvalbumin changes residual Ca^{2+} and converts paired-pulse depression to facilitation at this synapse (Caillard et al., 2000). It is important to note that lack of facilitation may be limited to P11–16 mice, and facilitation has been seen at more matured rat synapse (Pouzat and Hestrin, 1997). Nevertheless, the mechanistic explanation presented here may hold in other synapses, because lack of facilitation has been shown in GABAergic synapses at rat collicular cultures and hippocampal basket cell-granule cell synapse (Kirischuk et al., 2002; Hefft et al., 2002).

Readily Releasable Pool of Vesicles, the Rate of Vesicle Replenishment, and Synaptic Depression

The mechanisms of synaptic depression are diverse (Zucker and Regehr, 2002; Stevens, 2003). By measuring the RRP size and the rate of vesicle replenishment with flash photolysis and comparing the synaptic responses during an AP train, the present study indicates that the time course of synaptic depression can be explained by the rates of vesicle pool depletion and replenishment at the basket cell synapse (Figures 3, 5, and 6). A decrease in release probability (Betz, 1970; Wu and Borst, 1999) was not a dominant factor for depression in the present study, which can be caused by intrinsic heterogeneity of release probability (Hessler et al., 1993; Rosenmund et al., 1993), adaptation of release machinery (Hsu et al., 1996; Wolfel et al., 2007), and inactivation of presynaptic Ca^{2+} channels (Forsythe et al., 1998). Because flashes did not release more quanta than those observed during the initial phase of AP trains, reluctant vesicles, which are not released by APs, do not exist or constitute only a minor fraction at the basket cell synapse, consistent with GABAergic synapses in hippocampal cultures (Moulder and Mennerick, 2005). In other words, synaptic vesicles are efficiently recruited and used up during a train of APs at the basket cell synapse (''fire and reload''; Borges et al., 1995).

The time constant of vesicle replenishment ranges between several hundreds of milliseconds and several seconds, depending on the intracellular [Ca^{2+}] (Figure 3B). The value is slower than that of hair cell synapses (within 10 ms; Griesinger et al., 2005) and cerebellar mossy fiber and parallel fiber synapse (Saviane and Silver, 2006; Crowley et al., 2007), and it is faster than other synapses (several seconds; von Gersdorff et al., 1997; Stevens and Wesseling, 1998). An unexpected but important difference from other synapses is the requirement of high [Ca^{2+}]. At other synapses, vesicle replenishment is Ca^{2+} dependent but has a high affinity for [Ca^{2+}] (Dittman and Regehr, 1998; Stevens and Wesseling, 1998; Wang and Kaczmarek, 1998) or else Ca^{2+} dependence is not known. If the replenishment rate is constant, the rate of recovery from synaptic depression is as far as that of replenishment during an AP train (300–400 ms obtained by fitting the steady state; Figure 5A). However, the experimentally observed recovery time constant was much slower (1.7 s; Figure 6). A high-affinity Ca^{2+} sensor for replenishment predicts a slow recovery time course, but it also predicts that the steady-state amplitude becomes insensitive to the extracellular [Ca^{2+}] (Dittman and Regehr, 1998), which seems not to be the case at the basket cell synapse (Figure S6). The release model incorporating the requirement of high [Ca^{2+}] for replenishment predicts modulation of steady-state IPSC amplitude by changing the extracellular [Ca^{2+}] (Figure S6) as well as the slow recovery from depression (Figure 6). The mechanism observed here might be relevant at other synapses where the slow recovery is seen (Betz, 1970; Kusano and Landau, 1975).

The Coupling between Ca^{2+} Channels and Release Sites

At the basket cell terminals, local [Ca^{2+}] at the release site rises to a high level (20 μM) and falls rapidly (half-width of 0.5 ms) in response to an AP (Figure 4). The value is similar to some synapses (10–25 μM at the calyx of Held; Bollmann et al., 2000; Schneggenburger and Neher, 2000) but is lower than others (100 μM at squid giant synapses; Adler et al., 1991). Twenty μM [Ca^{2+}] could be reached by multiple Ca^{2+} channels with some distance from synaptic vesicles (Neher, 1998; Meinrenken et al., 2003). Local [Ca^{2+}] at the release site may change during development because release probability is known to decrease during development at basket cell (Pouzat and Hestrin, 1997) and other synapses (Bolshakov and Siegelbaum, 1995; Taschenberger and von Gersdorff, 2000).

For maintaining the steady-state IPSC amplitude during an AP train, >10 μM [Ca^{2+}] is required (see above). To obtain such a high [Ca^{2+}], the process of vesicle replenishment takes place closer to or even within the release site, compared with the synapses requiring lower [Ca^{2+}] for replenishment. In other words, it may be possible that vesicle replenishment studied here is not limited by translocation of vesicles but rather by vesicle priming in the same location. Landis and Reese (1974) have shown that basket cell-Purkinje cell synapse had no specialization of presynaptic components as seen in excitatory synapses, such as aggregates of small particles on presynaptic membrane. Aggregation of particles may represent active zone proteins (Gundelfinger et al., 2003) and are relevant for recruitment of synaptic vesicles to the active zones (Zenisek et al., 2000). The basket cell synapse may not require such an entry step as glutamatergic synapses do.

The Roles of Synaptobrevin in Transmitter Release at the Basket Cell Synapse

Molecular differences from excitatory synapses have been identified by cleaving synaptobrevin by BoNT/B and TeNT. Both toxins did not affect recovery from synaptic depression (Figure 7) or the vesicle replenishment rates (Figure 8). This differs from hippocampal synapses in culture (Deak et al., 2004) and the calyx of Held (Sakaba et al., 2005), where the vesicle replenishment rate was slowed by knockout or cleavage of synaptobrevin. It was also found that BoNT/B, but not TeNT, shifts the intracellular Ca^{2+} sensitivity. BoNT/B and TeNT cleave synaptobrevin at the same site (Gln 76-Phe 77), but TeNT binds at a more membrane-distal region (aa 38–47), whereas BoNT/B binds to a more membrane-proximal region (more toward the C terminus, aa 62–71; Pellizzari et al., 1996). In a cell-cell fusion assay system, BoNT/B, but not TeNT, can access and cleave trans-SNARE complexes (Giraudo et al., 2006). It has been shown that BoNT/B, but not TeNT, blocks fusion in a stimulation-independent manner at neuromuscular junctions, suggesting that the TeNT binding region is shielded when synaptic vesicles are docked (Hua and Charlton, 1999). However, it has not been shown at which time point of vesicle cycling the BoNT/B-binding site, but not the TeNT-binding site, is accessible, and the present study suggests that it is the time point of Ca^{2+} sensing and vesicle fusion. The finding is consistent with the notion that assembly of the SNARE complex begins at the N terminus of SNARE proteins, but further zippering is prevented before fusion, whereas final zippering of the C terminus is important for driving fusion (Giraudo et al., 2006; Sorensen et al., 2006). According to this view, BoNT/B is still accessible after docking reaction mediated by N-terminal SNAREs and compromises the kinetics of fusion. The data do not support the notion of SNARE complex formation as a concerted process as has been observed in PC12 cells (Han and Jackson, 2006). However, the present study

can also be compatible with other schemes (Arac et al., 2006; Stein et al., 2007), for example, the relevance of synaptobrevin C-terminal relevant for Ca^{2+} sensing. It is unknown whether BoNT/B shifts Ca^{2+} sensitivity at other synapses. At neuromuscular junctions, it was shown that impairment of synaptobrevin changes the slope of the relationship between external [Ca^{2+}] and quantal content (Bevan and Wendon, 1984; Stewart et al., 2000). The discrepancy with the present study showing no change in Ca^{2+} cooperativity may result from different preparations or may be due to an interaction of SNAREs and presynaptic Ca^{2+} channels in these studies (Jarvis and Zamponi, 2001).

Physiological Implications

It is important to note that this study was carried out in P11–16 mice at room temperature, and the release properties might change with development and temperature (Pouzat and Hestrin, 1997; Kuschmerick et al., 2006). Nevertheless, lack of reluctant vesicles (efficient vesicle replenishment to Ca^{2+} channels), altered Ca^{2+} sensitivity, and rapid sensing of Ca^{2+} signals by both vesicle fusion and replenishment processes seem to suggest that the basket cell synapse of P11–16 mice is designed to mediate precise synchronous release during an AP train and eliminate short-term plasticity except synaptic depression, while allowing asynchronous release in response to accumulation of bulk [Ca^{2+}]. Together with fast kinetics of release, relatively constant IPSC amplitude may allow for precise and rapid feedforward inhibition to Purkinje cells (Mittmann et al., 2005). The reduction of the steady-state synaptic strength could be achieved by modulation of presynaptic Ca^{2+} current amplitudes (Figure S5) through neuromodulators. This is in contrast to some glutamatergic synapses where the initial EPSC amplitude, but not the steady-state level, is sensitive to neuromodulators (Tsodyks and Markram, 1997; Brenowitz et al., 1998; Kreitzer and Regehr, 2000).

EXPERIMENTAL PROCEDURES

Electrophysiology and Flash Photolysis

Presynaptic and postsynaptic recordings at the basket cell-Purkinje cell synapse were performed using the acute slice preparation from P11–16 NMRI mice cerebellum (Vincent and Marty, 1996). The experiments were carried out according to the guidelines of German law on animal protection. Slices (200 μm in thickness) were cut in the vermis parallel to the sagittal plane. Slices were kept in an incubation chamber at 36°C for at least 1 hr and transferred to the recording chamber and perfused continuously with normal saline containing (in mM) NaCl 125, KCl 2.5, $CaCl_2$ 2, $MgCl_2$ 1, glucose 25, $NaHCO_3$ 25, Na_2Po_4 1.25, L-ascorbic acid 0.4, myo-inositol 3, and Na-pyruvate 2, pH 7.3–7.4, 320 mosm, and was bubbled continuously with 95% O_2 and 5% CO_2. During the recordings, the solution was supplemented with NBQX (2–10 μM) to block AMPA receptor-mediated EPSCs. In some experiments, TPMPA (300 μM), a low-affinity $GABA_A$ receptor antagonist (Jones et al., 2001), was applied to prevent receptor saturation. Because TPMPA may activate $GABA_B$ receptors (Ragozzino et al., 1996), CGP35348 (100 μM) was also applied. TPMPA may also activate $GABA_C$ receptors, which are also expressed in Purkinje cells (Harvey et al., 2006). A lower concentration of TPMPA (50 μM), which should sufficiently block $GABA_C$ receptors (Harvey et al., 2006), reduced an AP-evoked release to 80% ± 2.6% (n = 3 pairs). All experiments were carried out at room temperature (20°C–24°C) and within 5 hr after slicing.

Basket cells were identified by the position of the soma in the molecular layer, and the identification was confirmed by a long axon making collaterals to several Purkinje cell somas using Fura fluorescence (Figure 1 and Figure S1). Dendrites are much shorter, and the data were discarded if identification of the terminal was uncertain. Because Fura fluorescence coming from the soma may interfere with that of the terminal, usually a pair of basket and Purkinje cells with some distance to each other (30–200 μm) were selected for recording. Therefore, the probability for a connected pair was not high (30%). In our recording conditions, the Purkinje cell soma was innervated by a single axon terminal (Figure 1) or was wrapped by the terminals (Figure S1; Southan and Robertson, 1998). Because some cells show serious rundown of transmitter release, the analysis was restricted to the first 10 min after whole-cell rupture. During this period, beading of the axons was not serious. In order to allow quick diffusion of the Ca^{2+} indicator and the caged Ca^{2+} compound, their concentrations in the patch pipettes were relatively high as described below. Diffusion of compounds was monitored by Fura fluorescence, and 3–5 min were usually enough to start the experiments. Z axis of the objective was adjusted such that maximal fluorescence from the terminal could be obtained.

Presynaptic and postsynaptic compartments were simultaneously clamped at −80 mV using an EPC10/2 amplifier controlled by the Pulse Program (HEKA, Lambrecht, Germany). In some recordings, postsynaptic Purkinje cells were clamped at −100 mV. For postsynaptic recordings, the patch pipette (2–3 MΩ) contained (in mM) CsCl 170, HEPES 10, MgATP 4, NaGTP 0.3, EGTA 5, pH7.2, 320 mosm. The series resistance (4–8 MΩ) was compensated by the amplifier such that the residual resistance became 1.5–2.5 MΩ. The presynaptic pipette (4–6 MΩ) contained (in mM) KCl 130, KCl 20, HEPES 10, MgATP 5, NaGTP 0.5, EGTA 0.05–0.2, pH 7.2, 320 mosm. In the experiment of Figure S5, Fura-4F (0.5 mM) was included instead of EGTA. The presynaptic series resistance was typically 8–30 MΩ and was not compensated electrically. In order to elicit an AP escaped from voltage clamp, a voltage step (0 mV for 2 ms) was applied to the basket cells. A shorter step (1 ms) or an AP evoked by current injection under current-clamp mode evoked a similar IPSC amplitude (94% ± 11% and 94% ± 13%, respectively, from five cell pairs). Light chain of BoNT/B and TeNT was provided by Alexander Stein in the Department of Neurobiology, Max Planck Institute for Biophysical Chemistry, and was included into the presynaptic patch pipette.

A UV flash lamp (photolysis duration of 1 ms; Rapp, Hamburg, Germany) was used to elicit step-like elevations of [Ca^{2+}] in the presynaptic terminal as described in Schneggenburger and Neher (2000). In this study, presynaptic [Ca^{2+}] was monitored by Fura-2FF or Fura-4F (see also Llano et al., 1997; Forti et al., 2000), which was excited at 350/380 nm or 360/380 nm by a monochromator (Polychrome 4, Till Photonics, Gräfelfing, Germany). Fluorescence was collected by a CCD camera (VGA, Till Photonics, Gräfelfing, Germany). Monochromator and CCD camera were controlled by Tillvision software (Till Photonics, Gräfelfing, Germany). For Ca^{2+} measurements, images were binned by 4 × 4 pixels. Presynaptic patch pipettes contained (in mM) K-gluconate 80–110, KCl 20, HEPES 20, $MgCl_2$ 0.5, Na_2ATP 5, NaGTP 0.5, DM-nitrophen 1–10, $CaCl_2$ 0.85–8.5, Fura-2FF or Fura-4F 0.5–0.8, pH 7.2, 320 mosm. Presynaptic [Ca^{2+}] was derived from the ratiometric measurements. Calibration was performed in vitro, and R_{min} and $R_{intermediate}$ were confirmed by in vivo measurements at the calyx of Held.

Analysis

In order to estimate changes in quantal sizes during a train of presynaptic APs, nonstationary fluctuation analysis was used. The presynaptic basket cell was stimulated by an AP train (50 Hz × 20 times) with an interval of 10 s. Mean and variance were calculated for each IPSC amplitude during a train. The variance-mean plot was fitted by a line, and quantal sizes were estimated from the slope. To estimate the quantal sizes, the coefficient variation of mIPSC amplitudes (Figure 1C; CV = 0.86) and the fluctuation of latency of individual quantal events were taken into account (Taschenberger et al., 2005). In order to estimate the transmitter release rates, IPSCs were deconvolved with mIPSCs (Diamond and Jahr, 1995). Data are expressed as mean ± SEM.

Release Model

The relationship between [Ca^{2+}] and release rate per vesicle, time constants, as well as delays of transmitter release following flash photolysis (defined as the interval between the onset of flash and the time point when three vesicles have been released) were modeled by the five-site model developed by Schneggenburger and Neher (2000) connected to Ca^{2+}-dependent priming steps (The second scheme of Millar et al., 2005) as described below.

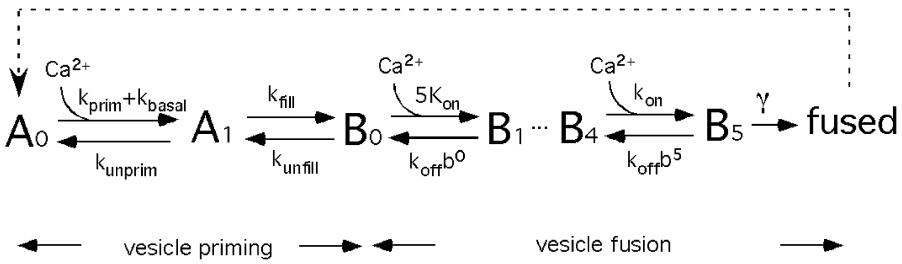

All parameters were found by trial and error using Euler integration. For priming reaction, a single Ca^{2+}-binding step is assumed, which is followed by a Ca^{2+}-independent step filling the RRP. Priming reaction operates only when the site becomes empty because of vesicle fusion (dotted line in the scheme). Once getting into B_0, vesicles are considered as readily releasable. The forward and backward rates of Ca^{2+}-dependent priming step are k_{prim} = 5×10^6 $M^{-1}s^{-1}$, $k_{unpriming}$ = 50 s^{-1}, respectively. Furthermore, basal priming rate of k_{basal} = 2 s^{-1} was introduced. The Ca^{2+}-independent filling rates are k_{fill} = 8 s^{-1} and k_{unfill} = 0.12 s^{-1}, respectively. The forward rate k_{on}, the backward rate k_{off}, cooperativity factor b, and the final rate γ are k_{on} = 9×10^7 $M^{-1}s^{-1}$, k_{off} = 3000 s^{-1}, b = 0.25, γ = 5000 s^{-1} in the control condition. In order to estimate the time course of local $[Ca^{2+}]$ evoked by a single AP, various amplitudes and time courses of $[Ca^{2+}]$ were entered into the release model until the release time course was perfectly predicted by the release model. The time course of residual $[Ca^{2+}]$ was varied until the model predicted the time course of asynchronous release during the train perfectly. In order to simulate the time course of release during an AP train, the $[Ca^{2+}]$ waveform evoked by a single AP was repeated during the train. In order to simulate the time course of depression, release probability evoked by a single AP was set to be 0.09 in 2 mM extracellular Ca^{2+}. In 1, 5, and 10 mM Ca^{2+} (but containing DM-nitrophen in 10 mM condition), it was estimated to be 0.015, 0.17, and 0.23, respectively. Experimentally, a single AP-evoked IPSC amplitude changes to 15% (Figure S6), 275% ± 100% (n = 3 cell pairs), and 334% ± 86% (n = 3 cell pairs), when the external Ca^{2+} was changed from 2 mM to 1, 5, and 10 mM, respectively.

Supplemental Data

The Supplemental Data for this article can be found online at http://www.neuron.org/cgi/content/full/57/3/406/DC1/.

ACKNOWLEDGMENTS

I thank Alexander Stein for suggestions and kindly providing BoNT/B and TeNT; and Erwin Neher for encouragement and advices throughout this work. I also thank Isabel Llano, Alain Marty, Tomoyuki Takahashi, Lu-Yang Wang, Ralf Schneggenburger, Ko Matsui, Nobutake Hosoi, and Kristian Wadel for helpful comments.

Received: January 27, 2007
Revised: September 23, 2007
Accepted: November 30, 2007
Published: February 6, 2008

REFERENCES

Abbott, L.F., Varela, J.A., Sen, K., and Nelson, S.B. (1997). Synaptic depression and cortical gain control. Science *275*, 220–224.

Adler, E.M., Augustine, G.J., Duffy, S.N., and Charlton, M.P. (1991). Alien intracellular calcium chelators attenuate neurotransmitter release at the squid giant synapse. J. Neurosci. *11*, 1496–1507.

Angleson, J.K., and Betz, W.J. (2001). Intraterminal Ca^{2+} and spontaneous transmitter release at the frog neuromuscular junction. J. Neurophysiol. *85*, 287–294.

Arac, D., Chen, X.C., Khant, H.A., Ubach, J., Ludtke, S.J., Kikkawa, M., Johnson, A.E., Chiu, W., Südhof, T.C., and Rizo, J. (2006). Close membrane-membrane proximity induced by Ca2+-dependent multivalent binding of synaptotagmin-1 to phospholipids. Nat. Struct. Mol. Biol. *13*, 209–217.

Auger, C., and Marty, A. (2000). Quantal currents at single-site central synapses. J. Physiol. *526*, 3–11.

Barrett, E.F., and Stevens, C.F. (1972). Quantal independence and uniformity of presynaptic release kinetics at the frog neuromuscular junction. J. Physiol. *227*, 665–689.

Betz, W.J. (1970). Depression of transmitter release at the neuromuscular junction of the frog. J. Physiol. *206*, 629–644.

Beutner, D., Voets, T., Neher, E., and Moser, T. (2001). Calcium dependence of exocytosis and endocytosis at the cochlear inner hair cell afferent synapse. Neuron *29*, 681–690.

Bevan, S., and Wendon, L.M. (1984). A study of the action of tetanus toxin at rat soleus neuromuscular junction. J. Physiol. *348*, 1–17.

Bolshakov, V.Y., and Siegelbaum, S.A. (1995). Regulation of hippocampal transmitter release during development and long-term potentiation. Science *269*, 1730–1734.

Bollmann, J.H., Sakmann, B., and Borst, J.G.G. (2000). Calcium sensitivity of glutamate release in a calyx-type terminal. Science *289*, 953–957.

Borges, S., Gleason, E., Turelli, M., and Wilson, M. (1995). The kinetics of quantal transmitter release from retinal amacrine cells. Proc. Natl. Acad. Sci. USA *92*, 6896–6900.

Borst, J.G.G., and Sakmann, B. (1998). Facilitation of presynaptic calcium currents in the rat brainstem. J. Physiol. *513*, 149–155.

Brenowitz, S., David, J., and Trussell, L. (1998). Enhancement of synaptic efficacy by presynaptic GABA(B) receptors. Neuron *20*, 135–141.

Caillard, O., Moreno, H., Schwaller, B., Llano, I., Celio, M.R., and Marty, A. (2000). Role of the calcium-binding protein parvalbumin in short-term synaptic plasticity. Proc. Natl. Acad. Sci. USA *97*, 13372–13377.

Crowley, J.J., Carter, A.G., and Regehr, W.G. (2007). Fast vesicle replenishment and rapid recovery from desensitization at a single synaptic release site. J. Neurosci. *27*, 5448–5460.

Cuttle, M.F., Tsujimoto, T., Forsythe, I.D., and Takahashi, T. (1998). Facilitation of the presynaptic calcium current at an auditory synapse in rat brainstem. J. Physiol. *512*, 723–729.

Deak, F., Schoch, S., Liu, X., Südhof, T.C., and Kavalali, E.T. (2004). Synaptobrevin is essential for fast synaptic-vesicle endocytosis. Nat. Cell Biol. *6*, 1102–1108.

Diamond, J.S., and Jahr, C.E. (1995). Asynchronous release of synaptic vesicles determines the time course of the AMPA receptor-mediated EPSC. Neuron *15*, 1097–1107.

Dittman, J.S., and Regehr, W.G. (1998). Calcium dependence and recovery kinetics of presynaptic depression at the climbing fiber to Purkinje cell synapse. J. Neurosci. *18*, 6147–6162.

Dittman, J.S., Kreitzer, A.C., and Regehr, W.G. (2000). Interplay between facilitation, depression, and residual calcium at three presynaptic terminals. J. Neurosci. *20*, 1374–1385.

Forsythe, I.D., Tsujimoto, T., Barnes-Davies, M., Cuttle, M.F., and Takahashi, T. (1998). Inactivation of presynaptic calcium current contributes to synaptic depression at a fast central synapse. Neuron *20*, 797–807.

Forti, L., Pouzat, C., and Llano, I. (2000). Action potential-evoked Ca^{2+} signals and calcium channels in axons of developing rate cerebellar interneurons. J. Physiol. *527*, 33–48.

Frerking, M., Borges, S., and Wilson, M. (1997). Are some minis multiquantal? J. Neurophysiol. *78*, 1293–1304.

Geiger, J.R.P., and Jonas, P. (2000). Dynamic control of presynaptic Ca2+inflow by fast-inactivating K+ channels in hippocampal mossy fiber boutons. Neuron *28*, 927–939.

Giraudo, C.G., Eng, W.S., Melia, T.J., and Rothman, J.E. (2006). A clamping mechanism involved in SNARE-dependent exocytosis. Science *313*, 676–680.

Goda, Y., and Stevens, C.F. (1994). Two components of transmitter release at a central synapse. Proc. Natl. Acad. Sci. USA *91*, 12942–12946.

Griesinger, C.B., Richards, C.D., and Ashmore, J.F. (2005). Fast vesicle replenishment allows indefatigable signaling at the first auditory synapse. Nature *435*, 212–215.

Gundelfinger, E.D., Kessels, M.M., and Qualmann, B. (2003). Temporal and spatial coordination of exocytosis and endocytosis. Nat. Rev. Mol. Cell Biol. *4*, 127–139.

Hagler, D.J., and Goda, Y. (2001). Properties of synchronous and asynchronous release during pulse train depression in cultured hippocampal neurons. J. Neurophysiol. *85*, 2324–2334.

Han, X., and Jackson, M.B. (2006). Structural transitions in the synaptic SNARE complex during Ca^{2+}-triggered exocytosis. J. Cell Biol. *172*, 281–293.

Harvey, V.L., Duguid, I.C., Krasel, C., and Stephens, G.J. (2006). Evidence that GABA {rho} subunits contribute to functional ionotropic GABA receptors in mouse cerebellar Purkinje cells. J. Physiol. *577*, 127–139.

Hefft, S., and Jonas, P. (2005). Asynchronous GABA release generates long-lasting inhibition at a principal interneuron-principal neuron synapse. Nat. Neurosci. *8*, 1319–1328.

Hefft, S., Kraushaar, U., Geiger, J.R.P., and Jonas, P. (2002). Presynaptic short-term depression is maintained during regulation of transmitter release at a GABAergic synapse in rat hippocampus. J. Physiol. *539*, 201–208.

Heidelberger, R., Heinemann, C., Neher, E., and Matthews, G. (1994). Calcium dependence of the rate of exocytosis in a synaptic terminal. Nature *371*, 513–515.

Hessler, N.A., Shirke, A.M., and Malinow, R. (1993). The probability of transmitter release at a mammalian central synapse. Nature *366*, 569–572.

Hsu, S.F., Augustine, G.J., and Jackson, M.B. (1996). Adaptation of Ca^{2+}-triggered exocytosis in presynaptic terminals. Neuron *17*, 501–512.

Hua, S.Y., and Charlton, M.P. (1999). Activity-dependent changes in partial VAMP complexes during neurotransmitter release. Nat. Neurosci. *2*, 1078–1083.

Jarvis, S.E., and Zamponi, G.W. (2001). Interactions between presynaptic Ca^{2+} channels, cytoplasmic messengers and proteins of the synaptic vesicle release complex. Trends Pharmacol. Sci. *22*, 519–525.

Jones, M.V., Jonas, P., Sahara, Y., and Westbrook, G.L. (2001). Microscopic kinetics and energetics distinguish GABAA receptor agonists from antagonists. Biophys. J. *81*, 2660–2670.

Katz, B., and Miledi, R. (1968). The role of calcium in neuromuscular facilitation. J. Physiol. *195*, 481–492.

Kirischuk, S., and Grantyn, R. (2002). Inter-bouton variability of synaptic strength correlates with heterogeneity of presynaptic Ca^{2+} signals. J. Neurophysiol. *88*, 2172–2176.

Kirischuk, S., and Grantyn, R. (2003). Intraterminal Ca2+ concentration and asynchronous transmitter release at single GABAergic boutons in rat collicular cultures. J. Physiol. *548*, 753–764.

Kirischuk, S., Veselovsky, N., and Grantyn, R. (1999). Relationship between presynaptic calcium transients and postsynaptic currents at single gamma-aminobutyric acid (GABA)ergic boutons. Proc. Natl. Acad. Sci. USA *96*, 7520–7525.

Kirischuk, S., Clements, J.D., and Grantyn, R. (2002). Presynaptic and postsynaptic mechanisms underlie paired pulse depression at single GABAergic boutons in rat collicular cultures. J. Physiol. *543*, 99–116.

Kraushaar, U., and Jonas, P. (2000). Efficacy and stability of quantal GABA release at a hippocampal interneuron-principal neuron synapse. J. Neurosci. *20*, 5594–5607.

Kreitzer, A.C., and Regehr, W.G. (2000). Modulation of transmission during trains at a cerebellar synapse. J. Neurosci. *20*, 1348–1357.

Kusano, K., and Landau, E.M. (1975). Depression and recovery of transmission at the squid giant synapse. J. Physiol. *245*, 13–32.

Kushmerick, C., Renden, R., and von Gersdorff, H. (2006). Physiological temperatures reduce the rate of vesicle pool depletion and short-term depression via an acceleration of vesicle recruitment. J. Neurosci. *26*, 1366–1377.

Landis, D.M.D., and Reese, T.S. (1974). Differences in membrane structure between excitatory and inhibitory synapses in the cerebellar cortex. J. Comp. Neurol. *155*, 93–126.

Llano, L., Tan, Y.P., and Caputo, C. (1997). Spatial heterogeneity of intracellular Ca2+ signals in axons of basket cells from rat cerebellar slices. J. Physiol. *502*, 509–519.

Llinas, R., Sugimori, M., and Silver, R.B. (1992). Microdomains of high calcium concentration in a presynaptic terminal. Science *256*, 677–679.

Lu, T., and Trussell, L.O. (2000). Inhibitory transmission mediated by asynchronous transmitter release. Neuron *26*, 683–694.

Maximov, A., and Südhof, T.C. (2005). Autonomous function of synaptotagmin 1 in triggering synchronous release independent of asynchronous release. Neuron *48*, 547–554.

Meinrenken, C.J., Borst, J.G., and Sakmann, B. (2003). Local routes revisited: the space and time dependence of the Ca^{2+} signal for phasic transmitter release at the rat calyx of Held. J. Physiol. *547*, 665–689.

Millar, A.G., Zucker, R.S., Ellis-Davies, G.C.R., Charlton, M.P., and Atwood, H.L. (2005). Calcium sensitivity of neurotransmitter release differs at phasic and tonic synapses. J. Neurosci. *25*, 3113–3125.

Mittmann, W., Koch, U., and Hausser, M. (2005). Feed-forward inhibition shapes the spike output of cerebellar Purkinje cells. J. Physiol. *563*, 369–378.

Moulder, K.L., and Mennerick, S. (2005). Reluctant vesicles contribute to the total readily releasable pool in glutamatergic hippocampal neurons. J. Neurosci. *25*, 3842–3850.

Neher, E. (1998). Vesicle pools and Ca^{2+} microdomains: new tools for understanding their roles in neurotransmitter release. Neuron *20*, 389–399.

Otsu, Y., Shahrezaei, V., Li, B., Raymond, L.A., Delaney, K.R., and Murphy, T.H. (2004). Competition between phasic and asynchronous release for recovered synaptic vesicles at developing hippocampal autaptic synapses. J. Neurosci. *24*, 420–433.

Pellizzari, P., Rossetto, O., Lozzi, L., Giovedi, S., Johnson, E., Schone, C.C., and Montecucco, C. (1996). Structural determinants of the specificity for synaptic vesicle-associated membrane protein/synaptobrevin of tetanus toxin and botulinm type B and G neurotoxins. J. Biol. Chem. *271*, 20353–20358.

Pouzat, C., and Hestrin, S. (1997). Developmental regulation of basket/stellate cellright-arrowPurkinje cell synapses in cerebellum. J. Neurosci. *17*, 9104–9112.

Ragozzino, D., Woodward, R.M., Murata, Y., Eusebi, F., Overman, L.E., and Miledi, R. (1996). Design and in vitro pharmacology of a selective gamma-aminobutyric acid(C) receptor antagonist. Mol. Pharmacol. *50*, 1024–1030.

Reyes, A., Lujan, R., Rozov, A., Burnashev, N., Somogyi, P., and Sakmann, B. (1998). Target-cell-specific facilitation and depression in neocortical circuits. Nat. Neruosci. *1*, 279–285.

Rieke, F., and Schwartz, E.A. (1996). Asynchronous transmitter release: control of exocytosis and endocytosis at the salamander rod synapse. J. Physiol. *493*, 1–8.

Rosenmund, C., Clements, J.D., and Westbrook, G.L. (1993). Nonuniform probability of glutamate release at a hippocampal synapse. Science *262*, 754–757.

Sakaba, T., Stein, A., Jahn, R., and Neher, E. (2005). Distinct kinetic changes in neurotransmitter release after SNARE protein cleavage. Science *309*, 491–494.

Saviane, C., and Silver, R.A. (2006). Fast vesicle reloading and a large pool sustain high bandwidth transmission at a central synapse. Nature *439*, 983–987.

Schneggenburger, R., and Neher, E. (2000). Intracellular calcium dependence of transmitter release rates at a fast central synapse. Nature *406*, 889–893.

Scheuss, V., Schneggenburger, R., and Neher, E. (2002). Separation of presynaptic and postsynaptic contributions to depression by covariance analysis of successive EPSCs at the calyx of Held synapse. J. Neurosci. *22*, 728–739.

Sorensen, J.B., Wiederhold, K., Muller, E.M., Milosevic, I., Nagy, G., de Groot, B.L., Grubmuller, H., and Fasshauer, D. (2006). Sequential N- to C-terminal SNARE complex assembly drives priming and fusion of secretory vesicles. EMBO J. *25*, 955–966.

Southan, A.P., and Robertson, B. (1998). Patch-clamp recordings from cerebellar basket cell bodies and their presynaptic terminals reveal an asymmetric distribution of voltage-gated potassium channels. J. Neurosci. *18*, 948–955.

Stein, A., Radhakrishnan, A., Riedel, D., Fasshauer, D., and Jahn, R. (2007). Synaptotagmin activates membrane fusion through a Ca^{2+}-dependent trans interaction with Phopholipids. Nat. Struct. Mol. Biol. *14*, 904–911.

Stevens, C.F. (2003). Neurotransmitter release at central synapses. Neuron *40*, 381–388.

Stevens, C.F., and Wesseling, J.F. (1998). Activity-dependent modulation of the rate at which synaptic vesicles become available to undergo exocytsois. Neuron *21*, 415–424.

Stewart, B.A., Mohtashami, M., Trimble, W.S., and Boulianne, G.L. (2000). SNARE proteins contribute to calcium cooperativity of synaptic transmission. Proc. Natl. Acad. Sci. USA *97*, 13955–13960.

Taschenberger, H., and von Gersdorff, H. (2000). Fine-tuning an auditory synapse for speed and fidelity: developmental changes in presynaptic waveform, EPSC kinetics, and synaptic plasticity. J. Neurosci. *20*, 9162–9173.

Taschenberger, H., Scheuss, V., and Neher, E. (2005). Release kinetics, quantal parameters and their modulation during short-term depression at a developing synapse in the rat CNS. J. Physiol. *568*, 513–537.

Thoreson, W.B., Rabl, K., Townes-Anderson, E., and Heidelberger, R. (2004). A Highly Ca^{2+}-sensitive pool of vesicles contributes to linearity at the rod photoreceptor ribbon synapse. Neuron *42*, 595–605.

Tsodyks, M.V., and Markram, H. (1997). The neural code between neocortical pyramidal neurons depends on neurotransmitter release probability. Proc. Natl. Acad. Sci. USA *94*, 719–723.

Tucker, T., and Fettiplace, R. (1995). Confocal imaging of calcium microdomains and calcium extrusion in turtle hair cells. Neuron *15*, 1323–1335.

Vincent, P., and Marty, A. (1996). Fluctuations of inhibitory postsynaptic currents in Purkinje cells from rat cerebellar slices. J. Physiol. *494*, 183–199.

von Gersdorff, H., Schneggenburger, R., Weis, S., and Neher, E. (1997). Presynaptic depression at a calyx synapse: the small contribution of metabotropic glutamate receptors. J. Neurosci. *17*, 8137–8146.

Wadel, K., Neher, E., and Sakaba, T. (2007). The coupling between synaptic vesicles and Ca^{2+} channels determines fast neurotransmitter release. Neuron *53*, 563–575.

Wang, L.Y., and Kaczmarek, L.K. (1998). High-frequency firing helps replenish the readily releasable pool of synaptic vesicles. Nature *394*, 384–388.

Wolfel, M., Lou, X., and Schneggenburger, R. (2007). A mechanism intrinsic to the vesicle fusion machinery determines fast and slow transmitter release at a large CNS synapse. J. Neurosci. *27*, 3198–3210.

Wu, L.G., and Borst, J.G. (1999). The reduced release probability of releasable vesicles during recovery from short-term synaptic depression. Neuron *23*, 821–832.

Zenisek, D., Steyer, J.A., and Almers, W. (2000). Transport, capture and exocytosis of single synaptic vesicles at active zones. Nature *406*, 849–854.

Zucker, R.S., and Regehr, W.G. (2002). Short-term synaptic plasticity. Annu. Rev. Physiol. *64*, 355–405.